

COVER PAGE

Document downloaded by @DAEL

Sat Nov 28 02:08:59 2026
For personal use

When automatic English translation is provided, only the original document is authentic.
The EAA cannot be held responsible of any translation error

Bibliographical reference

Flow Quantification in a Wall-Less Multiple Flow Phantom Using Ultrasound Plane Wave Doppler Imaging, David Lemonnier, Jean-Marc Mac-Thiong and Pierre Belanger, Acta Acustica **vol. 105** (Number 1), 2019, pp. 130-138

DOI
https://doi.org/10.3813/AAA.919294

Acta Acustica united with Acustica
Vol. 105 (2019) 130 – 138

Scientific Papers
DOI 10.3813/AAA.919294

Flow Quantification in a Wall-Less Multiple Flow Phantom Using Ultrasound Plane Wave Doppler Imaging

David Lemonnier[1,2], Jean-Marc Mac-Thiong[2,3,4], Pierre Belanger[1,2]

[1] École de technologie supérieure, Department of Mechanical Engineering, 1100 rue Notre-Dame Ouest, Montreal, QC H3C 1K3, Canada. pierre.belanger@etsmtl.ca

[2] Centre de recherche de l'Hôpital du Sacré-Cœur de Montréal, 5400 boulevard Gouin Ouest, Montreal, QC H4J 1C5, Canada

[3] Department of Surgery, Université de Montreal, 2900, boulevard Édouard-Montpetit, Montreal, QC H3T 1J4, Canada

[4] Department of Surgery, Hôpital Sainte Justine, 3175, chemin de la Côte-Sainte-Catherine, Montreal, QC H3T 1C4, Canada

Summary

Blood flow is a direct indicator of the spinal cord condition after an injury. Ultrasonic Doppler imaging is a portable, real-time modality which may be used to determine the spinal cord blood flow during surgery. Spinal cord blood flow may represent a particularly useful source of information for surgeons, it can be used to establish a diagnosis or to adapt the surgical procedure to be carried out. In this work, the flows measured respectively with a conventional focused algorithm generally included in clinical devices and from a plane wave sequence are compared. The properties of the imaging are based on an equivalent sampling frequency applied to a spinal cord vascularization phantom with a 10 MHz signal. The region of interest is calculated from the maximum value pixel in power Doppler images and used to determine the vessel diameters. The blood-mimicking fluid velocities are calculated using autocorrelation. A primary controlled flow was divided into several vessels inside wall-less phantoms. Three different configurations of vessels were studied. The vessel diameter was overestimated in all cases when using the focused algorithm, and as a result, the associated flow was almost twice as high as the actual values. The discrepancies in the flow division calculations were less than 5% with images reconstructed with plane waves. The results suggest that the blood flow inside small vessels can be more precisely estimated with ultrasound Doppler imaging using the plane wave algorithm. The distribution of the flow inside the vessels was also accurately estimated. This may allow the assessment of neurological functions following an injury and provide useful informations in other clinical issues such as cancer.

PACS no. 43.80.Ev, 43.80.Qf, 43.80.Vj

1. Introduction

Damage to the spinal cord after an injury can be particularly devastating as the spinal cord gathers many nervous terminations. Spinal cord injury leads to neurological impairment, and can strongly alter the quality of life. About 65 cases per million are seen in the United States [1] annually. The specific chronology of spinal cord blood flow (SCBF) after an injury was summarized in the literature [2]. Several authors find a general linear correlation between the severity of the injury and the SCBF at the impact site [3, 4, 5]. Blood flow is therefore a direct indicator of the spinal cord condition, and its quantification can be particularly interesting during spine surgeries as a useful aid for performing a diagnosis and predicting the consequences of the injury.

Currently, several techniques may be used to quantify the blood flow. The gas clearance and the radioactive microsphere techniques are the most commonly used quantification processes. The main limitation of these two procedures is that the values obtained reflect the global flow from a measured region, and as a result it is therefore impossible to describe the blood flow in specific vessels. Moreover, the intravenous injection of microspheres involves radioactive exposure. Magnetic Resonance Imaging (MRI), Computed Tomography (CT) scans and Positron Emission Tomography (PET) are some other tools used to quantify the blood flow. However, the bulky equipment required in these methods, as well as the need to ensure sterility while using them limit their use for in vivo applications. Laser Doppler is another powerful

Received 29 November 2017,
accepted 27 November 2018.

© S. Hirzel Verlag · EAA

imaging modality, but the quantification of blood flow using this technique is however restricted to measuring the velocity along only one dimension, with the measurement depth limited to only a few millimeters. Other techniques have been suggested in the literature, such as two photon microscopy [6], which is unfortunately limited to small animals because of limitations of depth for visualization.

Ultrasound imaging is one of the most widely used modalities to quantify blood flow. Its portable and real time nature allows its use during surgeries or other in vivo applications. The blood velocity calculated from the Doppler effect can be combined with the vessel diameter estimation obtained in a B-mode image to provide blood flow quantification [7]. The majority of the studies in the literature focus on large vessels viewed in a longitudinal plane. Moreover, contrast agents are frequently added to increase the signal and the image precision. Microbubbles injections are commonly used for that purpose [8, 9], but require additional steps.

Human spinal cord vessel diameters range from 1 mm, for the spinal arteries, down to 6 µm, for the capillaries [10, 11]. Such small vessels are extremely difficult to image correctly with the focused algorithm found in current clinical devices, and require very high signal frequencies. Plane wave ultrasound Doppler imaging was recently developed, and was initially applied to characterize the rat brain [12], after which it was used to quantify the flow in the heart [13, 14, 15] or in the carotid arteries [16, 17]. The imaging process activates all the probe elements to fully insonify the imaging plane for each emitted wave. The waves can be compounded to improve the signal-to-noise ratio of the images by insonifying from multiple angles [18]. As each probe element is activated at each emission, the energy transferred to the media is higher than for the focused algorithm for an equivalent time, as in the latter case only several piezoelectric elements are used to focus one ultrasound wave. Therefore, the sensitivity is improved and allows the quantification of vessels of smaller diameters. The ultrasound intensity may be closer to the safety limit defined by the U.S. Food and Drug Administration (FDA), but fortunately with plane waves the energy is not concentrated in a small area as it is the case with the focused waves algorithms. The ultrasound intensity can also be reduced by chosing a lower number of plane waves or a lower Pulse Repetition Frequency (PRF) if it is needed.

The spinal cord blood flow has however never been quantified using plane wave ultrasound Doppler imaging, from a representative phantom or during in vivo applications. In this work, a phantom design containing several vessel-like wall-less tubes simulating the size and flow of spinal cord vessels is firstly proposed. The flow through the phantom is quantified using plane wave Doppler ultrasound in a transverse plane, and compared with the flow calculated from focused waves. With the two algorithms, the imaging parameters were chosen according to in vivo imaging conditions of a human spinal cord. Several phantoms with multiple vessels in different configurations and with controlled flow were designed and compared. Secondly, the flow distribution inside the multiple vessels was also quantified and validated.

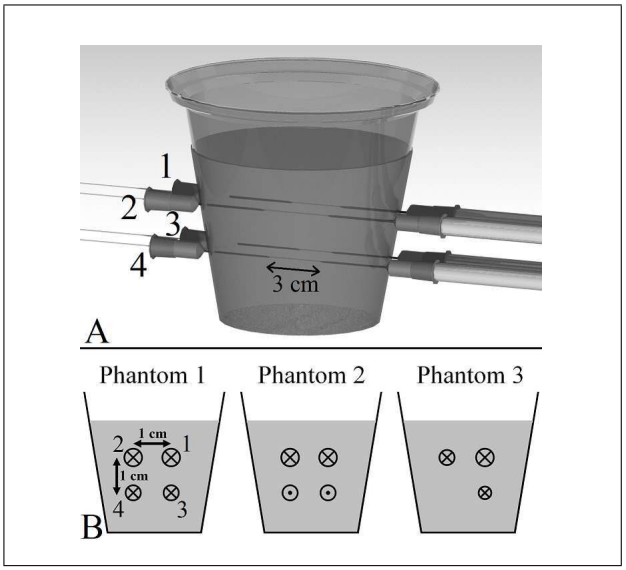

Figure 1. Phantom design principle, drawn in a longitudinal plane (A) and in a transverse plane for the three different configurations (B). The wires were guided with cylinders before the TMM was poured. After solidification of the TMM, the wires were pulled out of the phantom, thus creating empty tunnels simulating blood vessels. The experiments were performed with the probe on the solidified TMM surface. Inside the circles, the crosses and the dots represent the fluid flowing in opposite directions.

2. Methods

2.1. Phantom design

In this study, a wall-less Doppler flow phantom was designed, in order to eliminate artifacts caused by the use of tubes [19, 20]. Wires (fishing lines) corresponding to the desired blood vessel diameters were guided with metallic cylinders into each extremity of a plastic container (Figure 1), which is the same principle as that used in a previous study [21]. For each of the wires, three centimeters were not guided and were therefore left free in the middle of the phantom, and particular attention was paid to ensure that the wires were straight and parallel to the bottom of the container. Three different configurations were used to quantify the total flow inside the vessels, and they are summarized in Table I. For the two configurations with 4 flows, the vessels were included in two horizontal planes, each containing two vessels. All the guides and wires were separated to their two neighbors by a distance of 1 centimeter in a transverse plane. The same setup was used for the configuration with only three flows, with only one wire in the horizontal plane close to the bottom. The diameters were selected to represent the actual diameters found in the human spinal cord, as described previously. Moreover, these three phantom structures are in line with the main spinal cord vascular distribution, including three spinal arteries

Table I. Experimental configurations used in this study, included in three specific phantom patterns numbered in agreement with Figure 1. The values shown correspond to the diameter of the wires numbered in Figure 1. The blood-mimicking fluid (BMF) is flowing in the same direction in the four vessels for configurations 1 and 3. With configuration 2, the BMF inside the 0.7 mm vessels is flowing in an opposite direction to the 0.6 mm vessels.

	Diameter 1 (mm)	Diameter 2 (mm)	Diameter 3 (mm)	Diameter 4 (mm)
First configuration	0.7	0.7	0.6	0.6
Second configuration	0.7	0.7	0.6	0.6
Third Configuration	0.7	0.6	0.5	–

inside which blood flows along the spinal cord and in an opposite direction compared to the two spinal veins [2].

The tissue-mimicking material (TMM) used in this study is based on a previously published recipe [22]. This agar-based medium was liquid during the fabrication, and gelled at 36°C. The thimerosal added in the suggested composition, preventing a bacterial propagation, was replaced with 1 g of ethylenediaminetetraacetic acid (EDTA) due to experimental limitations. However, as the phantoms produced were not stored for a long period in our study, it is assumed that this modification did not alter the acoustical properties. The liquid medium was poured in the container with the wires and guides previously positioned as required, and then solidified at ambient temperature. Following this fabrication process, the phantom was placed in a refrigerator (T=6 °C) for one day to ensure it was completely solidified. Moreover, a layer of water was added on the top surface to prevent drying during storage. As the human spinal cord diameter ranges from 6 mm to 13 mm, depending on the vertebral level and the observation plane [23], a maximum depth of 19 mm was fixed to contain all of the vessels of the phantoms. The TMM thickness between the surface and the first wire was then adjusted to about 5 mm during the TMM pouring. As in vivo imaging of the spinal cord include a laminectomy which implies that only a gel thickness separates the transducer and the posterior surface of the spinal cord, this depth is representative of the spinal cord imaging conditions. Finally, the wires were carefully removed to create empty vessels inside the phantoms.

2.2. Experimental setup

The experimental setup is illustrated in Figure 2. Continuous flow was generated using a pump (Masterflex L/S Easy-load II, Cole-Parmer, Vernon Hills, IL, USA) with a maximum of 6 mL/min. The maximum flow was limited by the pump capabilities. The flow was chosen to obtain an identical theoretical mean velocity of 10 cm/s inside each of the vessels This velocity is in line with the results obtained in vivo for the human anterior spinal artery [24]. Calculations of the associated Reynolds number indicated that the flow was laminar even in the most restrictive cases, the velocity profile was then assumed to be parabolic. The mean velocity was calculated from the wire diameters used in the phantoms, assuming perfectly circular cross-sections and identical velocities inside each of the vessels. A compatible tube recommended by the manufacturer

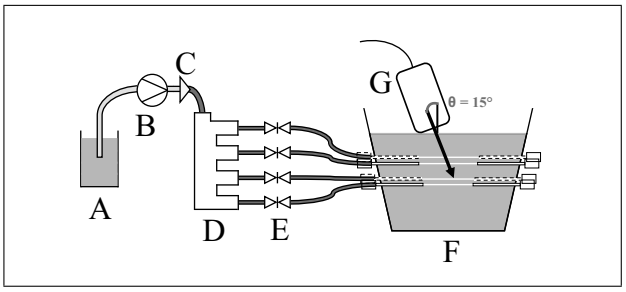

Figure 2. Experimental setup. A: Blood mimicking fluid, B: pump, C: tube adapter, D: manifold, E: Valves, F: phantom, G: probe, linked to the Verasonics acquisition system. The BMF is pumped from the container to the phantom with a flow controlled with the pump and the valves. With the second phantom configuration described in Table I, the phantom connections differ slightly with two tubes glued to the guides on each side.

(Masterflex L/S 13, Cole-Parmer, Vernon Hills, IL, USA) was used with the pump (light grey in Figure 2). One extremity was immersed into the blood-mimicking fluid (BMF) (Shelley Medical Imaging Technologies, London, ON, Canada) contained in a small container and regularly mixed to homogenize the 5 µm diameter nylon particles reflecting the ultrasound waves. The other end was connected to another tube (McMaster-Carr, Chicago, IL, USA), and then to a manifold (McMaster-Carr, Chicago, IL, USA), dividing the flow into four outlets. This second tube was used for all the remaining set-up (dark grey in Figure 2). High precision valves (McMaster-Carr, Chicago, IL, USA) connected to adapters (McMaster-Carr, Chicago, IL, USA) were placed between the manifold and the phantom guides, allowing to modify the flow distribution in the vessels in real time. It should be noted that prior to pouring the liquid TMM inside the phantom, the tubes were glued to the guides of one phantom extremity to avoid potential leakages, and were then plugged in the valves after removing the wires.

The ultrasound probe was positioned on top of the TMM surface, while ensuring that it did not compress the TMM surface and the underlying vessels. It was maintained with a holder, and kept in the same position for all experiments performed on a given phantom. The imaging plane was an oblique transversal plane compared to the flow direction, as shown in a previous study [25]. In order to get an impedance matching layer, the water layer was left on the surface of the phantom. An angle of approximately of 15° was chosen to avoid aliasing in the images

Table II. Wave emission parameters for both focused and plane wave algorithms.

	Plane wave Doppler	Focused Doppler
Wave frequency	10 MHz	10 MHz
Length of the emitted signal	2 cycles	2 cycles
Aperture	64 elements	26 elements
Focal length	–	10 mm
Steering	±5°	–
Imaging depth	19 mm	19 mm
Pulse Repetition Frequency	15380 Hz	15380 Hz
Doppler sampling frequency	3070 Hz	3070 Hz
Number of angles	5	–
Lines in a block	–	5
Number of blocks	–	13
Number of waves	1600	1600
Acquisition time	104 ms	104 ms
Ensemble length	320	25

and to simultaneously preserve the strength of the Doppler signal. Moreover, this value is representative of spinal cord surgery conditions, when only a narrow space is available to place the probe after a laminectomy, inducing a limitation for its possible orientation. This angle was determined more precisely from a photograph obtained in a plane perpendicular to the probe to convert the projected velocity given by the Doppler images.

2.3. Data processing

A Verasonics imaging system combined with the L11-4v transducer (Verasonics, Kirkland, USA) were used to perform ultrasound acquisitions. Experimental conditions limited the quantity of elements used in the probe to only the 64 central ones, leading to an image width of 19 mm. Plane wave and focused algorithms [12] were used alternatingly in order to limit temporal flow variations and to ensure comparable results. The algorithms parameters listed in Table II were chosen to obtain an equivalent Doppler sampling frequency for both imaging processes. Compared to the plane wave sequence, the ensemble length is thirteen times lower than with the focused sequence for the same imaging conditions and an equivalent acquisition time. High wave frequencies are required because of the very small diameters of vessels used in this work; the nominal frequency was therefore fixed to 10 MHz, which is close to the upper limit of the probe bandwidth. Consequently, the theoretical axial resolution was 0.15 mm. The input signal was a cosine taper burst 2 wavelengths long, and the sampling frequency was 25.7 MHz. For the two algorithms, the number of emissions was maximized to 1600 waves, leading to an acquisition time of 104 ms to get one Doppler image.

Tilted waves equally spaced between +5° and -5° were used to get a compound image with plane waves without limiting the insonified field. As the precise position of the created vessels may differ from one phantom to another, mainly following the liquid TMM pouring, the focal depth with the focused sequence was placed in the middle of the image corresponding to a value of 10 mm. This situation also reflect in vivo conditions, where the blood vessels´ positions are not perfectly known, and the anatomical conditions, such as the spinal cord diameter and the vessels´ pathway, differ among patients. No standard value exists for the F-number associated with the wave emission, an arbitrary value of 0.4 corresponding to 26 active elements was therefore chosen. Moreover, the imaging process was divided into a series of blocks in order to keep the same sampling frequency as the plane wave algorithm. Thirteen blocks containing five probe elements were then successively activated, which could have caused an offset between some lines in the image.

A time gain compensation (TGC) was added, followed by a demodulation process containing a 6th-order Butterworth low pass filter and a decimation. Beamforming was performed using a Delay and Sum calculation of the I/Q data. A 100 Hz 6th-order Butterworth clutter filter was then added, and to complete the processing step, a tapered window centered on the maximum value in the frequency domain was applied to reduce the effect of noise. For each pixel, the power Doppler image was finally calculated as the difference between the signal power in the positive part of the processed spectrum and its negative part, and the quantitative velocity was obtained from the phase difference calculated from an autocorrelation equation [26]:

$$\omega = \frac{1}{T} \arctan \left\{ \frac{\sum_{i=1}^{N} Q(i)I(i-1) - I(i)Q(i-1)}{\sum_{i=1}^{N} I(i)I(i-1) - Q(i)Q(i-1)} \right\}, \quad (1)$$

where ω is the angular frequency of the Doppler signal, T is the time between pulsed waves, and N is the number of samples. I and Q are the in-phase and quadrature signals obtained following the demodulation. As the flow direction is unique in a pixel, the other half of the Doppler spectrum is due to the noise.

2.4. Parameter control

The wire diameters were imaged with a confocal laser microscope (LEXT OLS4100, Olympus, Tokyo, Japan) and

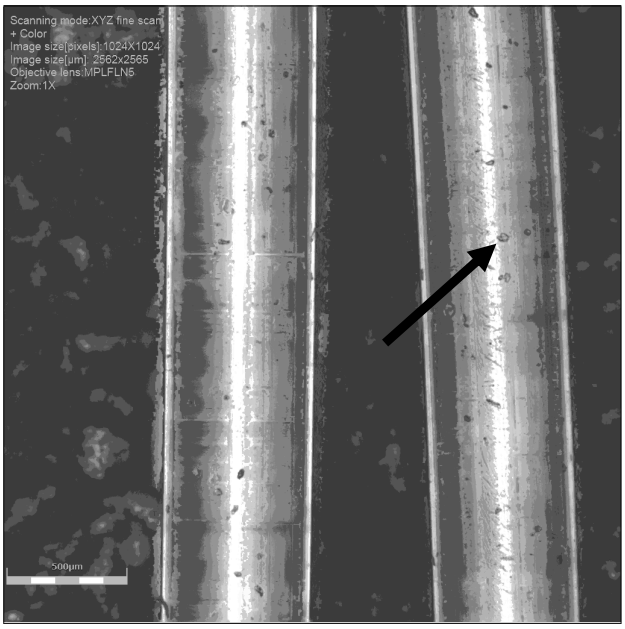

Figure 3. Laser microscope acquisition from theoretical 0.60 mm diameter wires. The defects, as indicated by the arrow on the figure, are supposed to have no effect on the actual vessel diameter inside the phantom.

compared with the expected values. As the wires were experimentally removed length-wise in the phantoms, the defects, which can be seen in the example given in Figure 3, were supposed to induce no modification on the actual vessel diameter inside the TMM. In order to quantify the actual wire diameters for each of the different calibers used in this study, several samples were fixed on a uniform background for each diameter. Following a segmentation process and calculations performed with the ImageJ software, a good diameter accuracy was obtained, with a maximum discrepancy of 3% in comparison with the expected values.

Control of the flow delivered by the pump is of critical importance in this study. For a requested flow of 6.00 mL/min used in the first two phantom configurations, a mean from five measurements performed over 30 minutes led to an actual flow of 5.28 mL/min . Similarly, an experimental value of 5.01 mL/min was obtained compared to the theoretical flow of 5.76 mL/min requested for the third phantom configuration. While the flows were underestimated in both cases, the difference was, however, respected. The BMF density calculation was also needed for the flow distribution experiments. From the fluid mass measured using an electronic balance (Symmetry PA220 Analytical Balance, Cole-Parmer, Vernon Hills, IL, USA) divided by the associated volume, the results revealed a mean density of 1012 kg/m^3.

The acoustic properties of the TMM were calculated from the mean of fourteen samples consisting of a TMM about 1 cm thick placed in a container, and carried out concurrently with the created phantoms. An electronic balance (type L310, Sartorius Laboratory, Goettingen, Germany) was used to measure the mass, and the volume was determined from the volume difference after immersing the sample in a scaled container (1 mL precision) filled with water. Finally, the speed of sound was obtained by dividing the sample thickness measured with a caliper (CD-6”CSX, Mitutoyo, Aurora, IL, USA) with the echo delay of an ultrasonic wave emitted from a probe placed perpendicularly to the surface. The acoustic impedance was calculated as the product of the density with the speed of sound in the TMM. While the measured (1004 kg/m^3) and theoretical water densities were similar, the speed of sound (1331 m/s) and the related acoustic impedance (1.34 MRayl) were however lower in comparison with the theoretical values of water (1480 m/s and 1.48 MRayl, respectively). The disparities in the speed of sound can be explained by variations of the pressures applied on the TMM during measurement, which may have caused its thickness values to differ slightly. Moreover, the plane containing the probe may not have been perfectly perpendicular to the phantom surface.

2.5. Quantification

In accordance with the most common method used in the literature on flow quantification using ultrasound imaging, the values obtained in this work were calculated by multiplying the vessel diameter, assumed to be circular, with the velocity. A region of interest (ROI) was defined for all the vessels in all the images, by selecting the maximum pixel value from every flow and then extending it to all of the surrounding pixels having a value greater than -6 dB from the maximum. This threshold is usually applied in signal processing [27, 28], and is equivalent to the full width at half maximum. It should be noted that all the images acquired with both algorithms contain the same number of pixels (158 in the probe width axis, 400 in the depth axis). The mean velocity is calculated as the mean value of the pixels inside the corresponding ROI from an autocorrelation equation. The associated diameter corresponds to the maximum width of the ROI linearly interpolated with the first neighbors in the probe length axis. The depth axis was not used to measure the diameter because of the distortion due to the angle between the probe and the phantom surface.

For each of the three phantom configurations, ten acquisitions were performed using the plane wave and the focused algorithms. A maximum of five images were obtained in each case in one phantom then at least two identical phantoms were used for each series of experiments to get ten acquisitions, which uncorrelates the results with the fabrication process variations. The total flow is the sum of the contributions from all of the vessels in one image, and the final flow for each of the phantom configurations was calculated as the mean of the total flow from the ten images.

For a second experiment, the flow distribution study was performed with the plane wave sequence and with a phantom containing two 0.7 mm and two 0.6 mm diameter vessels, all flowing in the same direction, corresponding to the

first configuration in Table I. Three different flow distributions were applied. With each case, an observation delay of one minute was added prior to the acquisitions to ensure that a steady state was established. For each distribution, the BMF was collected for a duration of 3 minutes in containers, and 3 acquisitions were performed during that time. As the phantom contained four vessels and three distributions were studied, twelve containers were used. The experimental flow was determined from mass measurements of each filled and empty container performed with an electronic balance (Symmetry PA220 Analytical Balance, Cole-Parmer, Vernon Hills, IL, USA), from the calculated BMF density calculated previously, and over the three-minute experimentation time. For each distribution, the experimental total flow was calculated as the sum of the individual corresponding flows from the four vessels. Similarly, the total flow values in the images associated with this distribution were determined as the sum of the four individual flows, with the calculation process described in this section, and then as the mean flow of the three reconstructed images. Finally, both flow calculation methods were relatively compared, for each of the three distributions studied.

3. Results

3.1. Diameters

The flow diameters were calculated from the reconstructed images, and the mean values for the three different phantoms and for both algorithms are summarized in Table III. The diameters were generally slightly underestimated using plane waves, with a maximum discrepancy of 0.12 mm (17%). The focused sequence always overestimated the diameters, whose disparities ranges from 0.22 mm to 0.33 mm, with standard deviations two to three times higher than the values obtained from the plane waves algorithm. As illustrated from power Doppler images reconstructions in Figure 4, the flows are more visible in the images reconstructed from the plane wave algorithm, as compared to the focused sequence, where more noise is present, and can be included in the ROI definition, therefore increasing its size. With the phantom containing two 0.7 mm and two 0.6 mm diameter vessels flowing in the same direction, the calculated diameters from the 0.6 mm vessels were slightly higher than the calculated diameters from the 0.7 mm vessels with both algorithms. Similarly, the estimated diameters from the 0.6 mm vessels were 0.02 mm lower than the calculated diameters from the 0.5 mm vessels, with the plane wave sequence and with the phantom containing the 0.7 mm, 0.6 mm and 0.5 mm diameter vessels.

3.2. Quantitative flow

The quantitative flow results are provided in Table IV. The plane waves algorithm slightly overestimates the total flow calculated from the first phantom, including 0.7 mm and 0.6 mm diameter vessels flowing in the same direction, and the results obtained in the images acquired from the two other configurations are contained inside the standard deviation range, which is always lower than 1.40 mL/min. The results are closer to the theoretical values for the second phantom configuration, containing with 0.7 mm and 0.6 mm diameter vessels flowing in opposite directions. With the focused sequence, the calculated flow is approximately two times higher than expected for the three different phantoms. The minimum standard deviation value of 2.35 mL/min is also greater in this case, and can reach up to 3.71 mL/min. In order to obtain ten images for each configuration, more images were removed due to undetected vessels with focused waves, showing more limitations in cases of low flow.

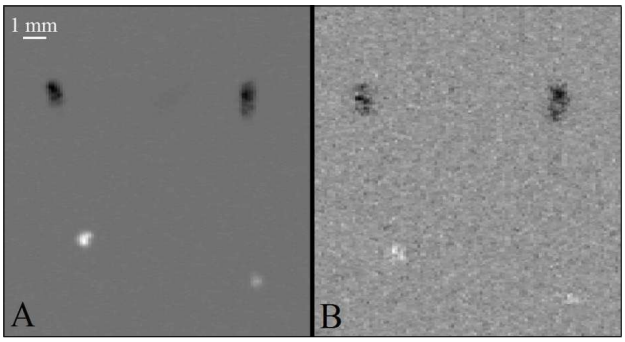

Figure 4. Power Doppler acquisitions using (A) the plane wave and (B) the focused algorithms, with the same experimental conditions, including the flow distribution. The four vessels are more apparent with the plane wave reconstruction due to a reduction of the noise.

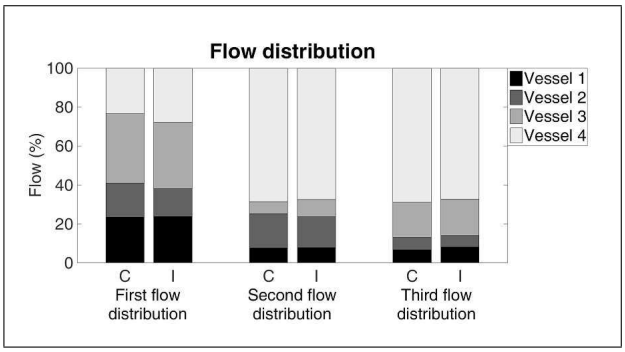

Figure 5. Relative flow division calculated from the reconstructed images (I in the figure) compared to the values determined from the harvested BMF volume in a container (C in the figure), with three different flow distributions. The experiments were performed using the plane wave algorithm in a phantom containing two 0.7 mm and two 0.6 mm diameter vessels flowing in the same direction. The results obtained with the two processes are close, with a maximum discrepancy of 4.4%. The results are given in percent.

3.3. Flow distribution

A flow distribution evaluation was performed using plane waves. The results obtained from the image calculations and from the BMF volume measured in the containers with the process detailed previously are given in Figure 5. As the total quantified flow may be slightly different using the

Table III. Mean diameters for each of the vessels in the three different phantoms. The values are given in mm, and the standard deviation is in brackets. The diameters are closer to the theoretical values with the plane waves algorithm, and with less disparities.

	First phantom configuration		Second phantom configuration		Third phantom configuration		
Theoretical diameter (mm)	0.7	0.6	0.7	0.6	0.7	0.6	0.5
Plane waves	0.61 (0.09)	0.62 (0.10)	0.58 (0.09)	0.52 (0.08)	0.62 (0.06)	0.57 (0.09)	0.59 (0.08)
Focused waves	0.92 (0.29)	0.93 (0.31)	0.94 (0.16)	0.86 (0.27)	0.95 (0.12)	0.86 (0.15)	0.79 (0.16)

Table IV. Mean flow calculated from ten reconstructed images with each of the three different phantoms and the two algorithms. The values are in mL/min and the standard deviation is written in brackets. A better accuracy is reached with plane waves compared to the focused algorithm, for which the flows are almost twice the theoretical values.

	First configuration	Second configuration	Third configuration
Theoretical flow	5.28	5.28	5.01
Plane waves	7.81 (1.39)	5.28 (1.32)	6.37 (1.37)
Focused waves	12.96 (3.41)	11.71 (2.35)	10.35 (3.71)

two methods, we used the normalized relative flow distribution for comparison. A maximum discrepancy of 4.4% was reached in the first experiment, when the four different flows were close to each other, and less than 3% with the two other situations.

4. Discussion

The non-invasive and real-time properties of ultrasound imaging are particularly useful for clinical applications. As a tissue condition and its associated vascular events are related following an injury, blood flow quantification is able to provide useful information during surgeries. The improvement of the small diameter vessel characterization using a plane wave Doppler imaging sequence as well as its comparison with the focused wave sequence has been previously studied [12, 18]. However, its efficiency to quantify the blood flow is not reported in the literature. The plane wave Doppler ultrasound imaging was also not applied to the spinal cord vascular conditions.

The flow calculation process performed in this work was similar to the most widely used ultrasound technique applied to quantify blood flow. The velocity and the flow quantifications were obtained from a transversal imaging plane with respect to the vessels [25], contrary to the more common approach in the literature which consists in visualizing the vessels in a longitudinal plane. This transversal imaging plane was needed in order to include several, not aligned vessels in the same image and to calculate the total flow. However, the velocity calculation process remains identical, based on the angle between the emitted ultrasound waves and the vessel axis. The insonification angle was limited to approximately 15° to take into account surgical conditions, where the available space to place the ultrasound transducer may be limited, for a contact with the spinal cord following a laminectomy.

With the plane waves technique adapted in the current study, the diameters are only slightly underestimated in all the phantoms and the theoretical diameter is generally included in the standard deviation range. In comparison, a large overestimation is observed with the focused sequence commonly found in current clinical devices. These results are in accordance to a previous study applied in similar experimental conditions [29]. The limited available data to generate the Doppler spectrum alters the power Doppler calculation accuracy with the focused sequence. Consequently, the shape of the vessel is not well defined, and can explain the highlighted discrepancies. Furthermore, more noise was observed, and can be included in the calculated ROI, increasing the vessel diameter in the images. The blooming artifact related to the power Doppler ultrasound imaging also presumably contributes to the flow diameter overestimation [30]. It is expected that the highlighted discrepancies will be reduced with an application using larger vessel diameters, as the vessel boundary variations should be similar, therefore providing a reduced overestimation compared to the diameter of the imaged vessel. Moreover, a spatial resolution limitation of the transducer should not longer exist with such applications.

These results are supported from a previous studies performed on a rat brain [12], where the application of the plane waves imaging sequence led to an improvement of the sensitivity by a factor 5 to 30, with a mean of 15. In addition, in the case of the carotid artery imaging [18] and for an equivalent acquisition time with both focused and plane waves algorithms, the image quality was significantly improved with the latter sequence and the variance was reduced. It should be noted that the spinal cord appli-

cation is a more restrictive situation due to the associated high flow velocities compared to these two studies. The increased number of blocks used in our experiments with the focused wave sequence may particularly cause more shifts in the image, affecting the vessel shape, and thus the diameter and the flow quantifications.

As a result, the calculated diameter variations are directly causing the flow overestimation with the focused waves, as this parameter is squared in the associated equation. Furthermore, with the two imaging sequences, a larger diameter may also be induced by the pressures caused by the BMF, distorting the vessel and increasing the cross-section. The total flow is close to the theoretical values with plane waves, with only a slight overestimation. This tendency was also observed in a previous study by comparing the blood flow obtained from ultrasound imaging to MR angiography measurements [30]. Experimentally, the difficulty to deliver a perfectly continuous flow with the pump can also contribute to minor total flow variability.

Currently, only a limited number of systems provide plane wave Doppler algorithms, as they requires fundamental changes in the imaging sequence. The amount of data as well as the computing time are also significantly higher, limiting the use of these algorithms in real time. Moreover, as the Doppler insonification angle is a critical variable for precisely estimating the blood flow from ultrasound imaging quantification, a precise knowledge of the vascular anatomy may also be required in order to interpret the results, due to the natural vascular complexity and variability of the vessels´ arrangement. Unfortunately, it is experimentally difficult to design an ultrasound Doppler phantom with a complex geometry or with many branches while using small vessels diameters. For a spinal cord application, an approximation could be to consider the spinal arteries and the spinal veins flowing longitudinally to the spinal cord. If the central arteries have to be characterized, the angle formed with the anterior spinal artery differs according to the vertebral level studied and is descibed in the literature [31]. Flow variation due to cardiac and respiratory cycles are also possible, but were not taken into account in the current study; nevertheless, these variations can be avoided by adding a trigger for the in vivo measurements or by fixing the probe holder to the surrounding vertebras [32] during in vivo applications.

5. Conclusion

The quantification of the blood flow with ultrasound imaging may be a powerful asset for the surgeon, as it is linked to the condition of the biological system studied. However, in the case of small blood vessels, the conventional focused waves algorithm may not be precise enough to quantify the associated vascularization. In the case of small vessels with diameters smaller than 1 mm, the plane wave algorithm only slightly overestimates the total flow, while it is almost doubled with a conventional focused sequence. Different flow distributions could be studied through valves included in the set-up, showing less than 5% discrepancies in the flow distribution quantification calculated from the reconstructed images using plane waves, which can therefore measure small flow variations and is suitable for use in a diagnosis based on vascular events.

Acknowledgements

The authors acknowledge Guy Rousseau for the material used in this study to create the phantoms, and Anthony Moulins for the Laser microscope acquisitions. This work was supported by a Natural Sciences and Engineering Research Council of Canada (NSERC) Discovery grant.

References

[1] N. B. Jain, G. D. Ayers, E. N. Peterson, M. B. Harris, L. Morse, K. C. O'Connor, E. Garshick: Traumatic spinal cord injury in the United States, 1993-2012. J Am Med Assoc **313** (2015) 2236–43.

[2] N. L. Martirosyan, J. S. Feuerstein, N. Theodore, D. D. Cavalcanti, R. F. Spetzler, M. C. Preul: Blood supply and vascular reactivity of the spinal cord under normal and pathological conditions. J Neurosurg Spine **15** (2011) 238–51.

[3] M. G. Fehlings, C. H. Tator, R. D. Linden: The relationships among the severity of spinal cord injury, motor and somatosensory evoked potentials and spinal cord blood flow. Electroencephalogr Clin Neurophysiol **74** (1989) 241–59.

[4] A. Guha, C. H. Tator, J. Rochon: Spinal cord blood flow and systemic blood pressure after experimental spinal cord injury in rats. Stroke **20** (1989) 372–7.

[5] Y. Zhang, S. Hou, R. Liu, Y. Zhu: Relationship between spinal cord blood flow and functional damage in acute spinal cord injury. Chinese Journal of Spine and Spinal Cord **5** (1999) 260–263.

[6] P. Tang, Y. Zhang, C. Chen, X. Ji, F. Ju, X. Liu, W. Gan, Z. He, S. Zhang, W. Li, L. Zhang: In vivo two-photon imaging of axonal dieback, blood flow, and calcium influx with methylprednisolone therapy after spinal cord injury. Sci. Rep. (2015) 1–10.

[7] P. Hoskins: Measurement of arterial blood flow by doppler ultrasound. Clin Phys Physiol Meas. **11** (1990) 1–26.

[8] K. Wei, A. Jayaweera, S. Firoozan, A. Linka, D. Skyba, S. Kaul: Quantification of myocardial blood flow with ultrasound-induced destruction of microbubbles administered as a constant venous infusion. Circulation **97** (1998) 473–483.

[9] C. Greis: Quantitative evaluation of microvascular blood flow by contrast-enhanced ultrasound (CEUS). Clinical Hemorheology and microcirculation **49** (2011) 137–149.

[10] T. H. Suh, L. Alexander: Vascular system of the human spinal cord. Arch NeurPsych **41** (1939) 659–677.

[11] G. J. Romanes: The arterial blood supply of the human spinal cord. Paraplegia **2** (1965) 199–207.

[12] E. Macé, G. Montaldo, B. F. Osmanski, I. Cohen, M. Fink, M. Tanter: Functional ultrasound imaging of the brain: theory and basic principles. IEEE Trans Ultrason Ferroelectr Freq Control **60** (2013) 492–506.

[13] B. F. Osmanski, M. Pernot, G. Montaldo, A. Bel, E. Messas, M. Tanter: Ultrafast doppler imaging of blood flow dynamics in the myocardium. IEEE Trans Med Imaging **31** (2012) 1661–8.

[14] B. F. Osmanski, G. Montaldo, M. Tanter: Out-of-plane doppler imaging based on ultrafast plane wave imaging. IEEE Trans Ultrason Ferroelectr Freq Control **62** (2015) 625–36.

[15] B. Denarie, T. A. Tangen, I. K. Ekroll, N. Rolim, H. Torp, T. Bjastad, L. Lovstakken: Coherent plane wave compounding for very high frame rate ultrasonography of rapidly moving targets. IEEE Trans Med Imaging **32** (2013) 1265–76.

[16] J. Flynn, R. Daigle, L. Pfulgrath, K. Linkhart, P. Kaczkowski: Estimation and display for vector doppler imaging using planewave transmissions. 2011 IEEE International Ultrasonics Symposium, 2011, IEEE, 413–8.

[17] I. K. Ekroll, A. Swillens, P. Segers, T. Dahl, H. Torp, L. Lovstakken: Simultaneous quantification of flow and tissue velocities based on multi-angle plane wave imaging. IEEE Trans Ultrason Ferroelectr Freq Control **60** (2013) 727–38.

[18] J. Bercoff, G. Montaldo, T. Loupas, D. Savery, F. Mézière, M. Fink, M. Tanter: Ultrafast compound doppler imaging: providing full blood flow characterization. IEEE Trans Ultrason Ferroelectr Freq Control **58** (2011) 134–147.

[19] D. W. Rickey, P. A. Picot, D. A. Christopher, A. Fenster: A wall-less vessel phantom for doppler ultrasound studies. Ultrasound Med Biol **21** (1995) 1163–76.

[20] T. L. Poepping, H. N. Nikolov, M. L. Thorne, D. W. Holdsworth: A thin-walled carotid vessel phantom for doppler ultrasound flow studies. Ultrasound Med Biol **30** (2004) 1067–78.

[21] S. Z. Pinter, J. C. Lacefield: Detectability of small blood vessels with high-frequency power doppler and selection of wall filter cut-off velocity for microvascular imaging. Ultrasound Med Biol **35** (2009) 1217–28.

[22] E. L. Madsen, G. R. Frank, F. Dong: Liquid or solid ultrasonically tissue-mimicking materials with very low scatter. Ultrasound Med Biol **24** (1998) 535–42.

[23] H. Y. Ko, J. H. Park, Y. B. Shin, S. Y. Baek: Gross quantitative measurements of spinal cord segments in human. Spinal Cord **42** (2004) 35–40.

[24] C. A. Giller, S. S. Finn: Intraoperative measurement of spinal cord blood velocity using pulsed doppler ultrasound. a case report. Surg Neurol **32** (1989) 387–93.

[25] B. Ihnatsenka, A. P. Boezaart: Ultrasound : Basic understanding and learning the language. Int. J. Shoulder Surg. **4** (2010) 55–62.

[26] C. Kasai, K. Namekawa, A. Koyano, R. Omoto: Real-time two-dimensional blood flow imaging using an autocorrelation technique. IEEE Transactions on sonics and ultrasonics **3** (1985) 458–464.

[27] S. Webb: The physics of medical imaging. Vol. 193. CRC Press, 1988, book 7.

[28] Ultrasonics – pressure pulse lithotripters – characteristics of fields. Standard International Electrotechnical Commission, Geneva, CH, apr 1998.

[29] D. Lemonnier, J. M. Mac-Thiong, P. Belanger: Ultrasound plane wave Doppler quantification using a wall-less spinal cord representative phantom. Acta Acust United Acust **104** (2018) 166–173.

[30] S. Oktar, C. Yücel, D. Karaosmanoglu, K. Akkan, H. Ozdemir, N. Tokgoz, T. Tali: Blood-flow volume quantification in internal carotid and vertebral arteries: comparison of 3 different ultrasound techniques with phase-contrast MR imaging. Am. J. Neuroradiol. **27** (2006) 363–369.

[31] R. Herren, L. Alexander: Sulcal and intrinsic blood vessels of human spinal cord. Arch NeurPsych **41** (1939) 678–687.

[32] M. Soubeyrand, E. Laemmel, A. Dubory, E. Vicaut, C. Court, J. Duranteau: Real-time and spatial quantification using contrast-enhanced ultrasonography of spinal cord perfusion during experimental spinal cord injury. Spine **37** (2012) 1376–1382.